Journal of Power Sources 194 (2009) 515–519

Contents lists available at ScienceDirect

Journal of Power Sources

journal homepage: www.elsevier.com/locate/jpowsour

Template-free reverse micelle process for the synthesis of a rod-like $LiFePO_4$/C composite cathode material for lithium batteries

Bing-Joe Hwang[a,c,*], Kuei-Feng Hsu[b], Shao-Kang Hu[a], Ming-Yao Cheng[a], Tse-Chuan Chou[b], Sun-Yuan Tsay[b], Raman Santhanam[d]

[a] Department of Chemical Engineering, National Taiwan University of Science & Technology, 43 Keelung Road, Sec. 4, Taipei 106, Taiwan
[b] Department of Chemical Engineering, National Cheng Kung University, No.1, Ta-Hsueh Road, Tainan 701, Taiwan
[c] National Synchrotron Radiation Research Center, Hsinchu 300, Taiwan
[d] Nanoexa Corporation, Burlingame, CA, USA

ARTICLE INFO

Article history:
Received 17 December 2008
Received in revised form 11 March 2009
Accepted 8 May 2009
Available online 20 May 2009

Keywords:
Li ion battery
$LiFePO_4$
$LiFePO_4$/C
Reverse micelle
Carbonization
Cathode

ABSTRACT

The synthesis of rod-like $LiFePO_4$/C cathodes using template-free reverse micelle process is reported for high performance lithium batteries. We have demonstrated that the size of the primary particles could be controlled based on sintering temperature and sintering time and size of the large aggregates is adjustable based on the carbon content of the sample. Thermogravimetry and differential thermal analysis have been used to propose a possible mechanism for the formation rod-like $LiFePO_4$/C cathode material. X-ray diffraction, scanning electron microscopy, impedance spectroscopy and charge–discharge measurements have been used to characterize the material. Electrochemical performance of rod-like $LiFePO_4$/C cathode material offers higher initial capacity and excellent rate capability than that obtained by loose porous $LiFePO_4$/C material due to unique rod-like composite material formed by primary nanoparticles. Hence, it can be suggested that that the rod-like nanostructured morphology improves structural stability, lithium ion diffusion and electronic conductivity of the $LiFePO_4$/C composite material. The template-free reverse micelle process for the synthesis of the rod-like $LiFePO_4$/C cathode material opens up a new route to synthesize lithium transition metal oxides with controlled morphologies for applications in high power lithium batteries.

1. Introduction

There has been great interests in developing lithium ion batteries with high energy/power density, high safety, long cycle life as well as low cost for applications in implantable medical devices, portable electronic devices and electric vehicles [1–4]. Among the several materials under development for use as cathode material for lithium ion batteries, olivine-type $LiFePO_4$ proposed by Goodenough and his co-workers [5,6] is particularly attractive because of its economic advantages, environmental friendliness, good thermal stability, flat voltage profile and non-toxicity. Although $LiFePO_4$ possesses so many advantages, the major drawback of this cathode material has been the low capacity achievable at even moderate discharge rates due to its slow lithium ion diffusion, poor electronic conductivity and slow interface movement of the $LiFePO_4$–$FePO_4$ two phase interface [5,7]. Many research groups have focused their efforts on improving electronic conductivity of olivine-type $LiFePO_4$ material. Great improvements have been achieved by carbon coating around the particles with different carbon sources [8–10], cation doping into the olivine structure [11–13], and minimizing the particle size by different synthetic processes [13–16]. Various synthesis methods have been proposed to prepare $LiFePO_4$ such as hydrothermal process [13], sol–gel method [15], solid state reaction [17], polyol process [18], mechanical alloying [19], microemulsion [20], spray solution technology [21], vapor deposition [22], co-precipitation [23] and so on. However, most of the methods reported were either high cost or not suitable for large-scale production due to complicated synthesis procedure.

The general approach for the synthesis of nanostructured $LiFePO_4$ has involved the use of various traditional methods such as hydrothermal [13], sol–gel [15] and co-precipitation [23]. Moreover, the reverse micelle process has long been established that surfactant molecules can self-assemble to form various ordered structures in nanometer scale [24,25]. Martin and co-workers have reported a series of studies on the nanostructured electrodes synthesized by using the template synthesis method to improve the rate capability and energy density [26–28]. However, nanostructured electrode materials prepared from template synthesis routes

* Corresponding author at: Department of Chemical Engineering, National Taiwan University of Science & Technology, 43 Keelung Road, Sec. 4, Taipei 106, Taiwan. Tel.: +886 2 27276624.
E-mail address: bjh@mail.ntust.edu.tw (B.-J. Hwang).

0378-7753/$ – see front matter © 2009 Elsevier B.V. All rights reserved.
doi:10.1016/j.jpowsour.2009.05.006

use polycarbonate filtration membranes followed by removal of membranes. Thus, template synthesis method suffers from disadvantages related to high cost and complicated synthetic procedures that are difficult to expand to large-scale commercial applications. Therefore, it is indeed essential to develop economic and efficient synthesis methods for the practical application of $LiFePO_4$ cathode material in rechargeable lithium batteries. Ideally one would prefer a template-free synthesis to prepare nanostructured materials in a wide range of sizes and shapes under controlled conditions.

Herein, we report a template-free reverse micelle process to synthesize a dense rod-like $LiFePO_4$/C composite material. The synthesis is performed in water–oil mixture using Tween#80 as the surfactant. In reverse micelle system, water droplets are dispersed separately in a continuous oil phase and acting as nanoreactors for the formation of nanoparticles for prevention of aggregation. The size of the particles is determined by the size of these water droplets. Since the synthesis is confined to the water droplet, the shapes of the nanomaterials synthesized with reverse micelle process were mostly spherical or quadrate or polyhedral. In this paper, however, we described a low cost and high yield template-free process for the production of rod-like $LiFePO_4$/C composite material. This as-prepared rod-like material exhibit highly improved electrochemical performance when used as a cathode material in lithium batteries.

2. Experimental

An aqueous solution was prepared with equimolar $LiNO_3$, $NH_4H_2PO_4$ and $Fe(NO_3)_3$. $9H_2O$ dissolving in distilled water with continuously mixing for 12 h. An oil mixture was prepared separately by mixing Tween#80 with kerosene, and stirred vigorously for 24 h. Tween#80 (a non-ionic surfactant and an emulsifier) was used as carbon source in this work. The aqueous solution was then added to the oil mixture at a rate of one droplet per second, and was stirred at high speed with an impeller to produce an emulsion. The precursors thus obtained were calcined at 650 °C at a heating rate of 3 °C min^{-1} for various holding times (0.5–20 h) in flowing N_2 for synthesizing $LiFePO_4$/C composite. The amount of carbon was determined by Heraeus CHN-O rapid analyzer which was calculated as 15.1 wt%. The thermal decomposition behavior of the gel precursor was examined by thermogravimetry analysis (TGA, PerkinElmer, TAC 7/DX) ranging from 50 to 800 °C at a heating rate of 5 °C min^{-1} with flowing N_2. The XRD patterns of the samples were acquired with an X-ray diffractometer (Rigaku Rotaflux) using Cu Kα radiation to confirm the phase purity. The surface morphology of the powders after calcination was characterized with a field emission-scanning electron microscope (JEOL, JSM-6700F).

Electrochemical characterization was carried out with coin-type cell. The electrode was prepared by using 80 wt% of $LiFePO_4$/carbon active material, 10 wt% Super P carbon black, and 10 wt% (PEO), as binder, dissolved in N-methyl-2-pyrrolidinone (NMP) solvent. The obtained slurry was then cast on the Al current collector and dried for 2 h in an oven at 100 °C. The resulting electrode film was subsequently pressed and punched into a circular disc. The thickness and loading of the electrode film were ~10 μm and ~1.0 mg cm^{-2}, respectively. The coin cell was fabricated using the lithium metal as a counter electrode. The electrolyte was 1 M solution of $LiPF_6$ in a mixture 1:1 (v/v) of ethylene carbonate (EC) and diethyl carbonate (DEC). The separator (Celgard 2400, Hoechst Celenese Corp) was soaked in an electrolyte for 24 h prior to use. Coin cell assembly was carried out in an argon-filled glove box (Unilab, Mbruan) by keeping both oxygen and moisture level less than 1 ppm. The charge–discharge measurements were performed using the programmable battery tester (Maccor 2300) at the controlled C-rate over a potential range between 3.0 V and 4.0 V. The impendence spectra of the coin cell were analyzed in the frequency range between 1 Hz and 100 kHz. The pre-equilibrium time was regulated to ensure that equilibrium conditions were reached.

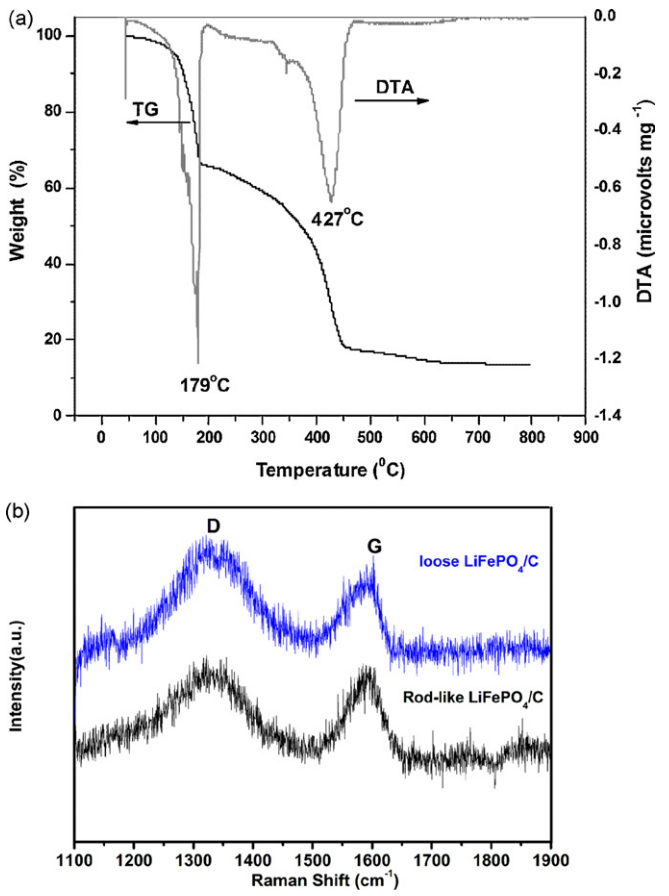

Fig. 1. (a) TG–DTA curves of reverse micelle containing $LiNO_3$, $NH_4H_2PO_4$, $Fe(NO_3)_3$, Tween 80 and kerosene recorded from ambient to 800 °C with a heating rate of 5 °C min^{-1} under nitrogen atmosphere and (b) Raman spectra of loose porous and rod-like $LiFePO_4$/C composite cathode materials.

3. Results and discussion

Typical thermogravimetric–differential thermal analysis (TG–DTA) results of a aqueous–oil mixture containing $LiNO_3$, $NH_4H_2PO_4$, $Fe(NO_3)_3$, Tween 80 (non-ionic surfactant and emulsifier) and kerosene are exhibited in Fig. 1. It exhibits several weight loss steps in the results. The first weight loss between 50 and 180 °C and the corresponding endothermic DTA peak at 179 °C indicate the vaporization of water and kerosene together with the decomposition of NO_3^- ions. In this stage, the salts were surrounded by the Tween 80. A continuous second weight loss between 180 and 450 °C and the corresponding endothermic DTA peak at 427 °C can be related to the decomposition of $NH_4H_2PO_4$ and pyrolysis of Tween 80. In this weight loss stage, the Li^+, Fe^{3+} and PO_4^{3-} were surrounded by the pyrolysis carbon and the Fe^{3+} ions began to reduce to Fe^{2+}. Note that when the heating temperature increases to the formation temperature of $LiFePO_4$ (400–450 °C) [15], the pyrolysis carbon becomes to act as the chelating agent to bridge amorphous $LiFePO_4$ for formation of the $LiFePO_4$/C composite network. Subsequently, the weight loss in the temperature range from 450 to 650 °C is not only due to the burning out of the pyrolysis carbon but also due to the structural change of the pyrolysis carbon. During this weight loss region, the soft amorphous hydrocarbon may form in the range of 400–600 °C but it transforms to hard carbon at temperature higher

than 600 °C [29]. The carbon transformation process results in a interesting structural change in the $LiFePO_4$/C composite material. As the sintering temperature increasing to hard carbon formation temperature (>600 °C), the carbon within $LiFePO_4$/C composite transfers to hard carbon and causes the volume shrinkage. Raman spectroscopy measurements were also carried out to detect the difference in the carbon formed on different $LiFePO_4$/C composite materials. Fig. 1b shows the Raman spectra of loose porous and rod-like $LiFePO_4$/C composite materials synthesized at 650 °C at two different sintering conditions, 2 and 20 h. The bands observed at ~1600 cm^{-1} and ~1330 cm^{-1} are the said graphitic band (G-band) and the disorder-induced phonon mode (D-band), respectively. The G- and D-bands are characteristic of carbon materials with larger degree of ordered structure and with disordered structure, respectively. The intensity ratio (I_D/I_G) provides information about the crystallinity of the carbon materials, i.e., smaller the ratio, higher the degree of ordering of the material. In this work, the I_D/I_G ratio of rod-like $LiFePO_4$/C composite material is relatively smaller than that of the loose porous material which indicates relatively a high degree of ordering in the carbon coated on rod-like $LiFePO_4$/C composite material. X-ray diffraction patterns (XRD) of the $LiFePO_4$/C composite materials synthesized at 650 °C at two different sintering conditions, 2 and 20 h, are shown in Fig. 2. The diffraction peaks of the materials are identified as the $LiFePO_4$ olivine crystalline structure indexed by orthorhombic *pnmb*. Impurity phases such as Li_3PO_4 and others were not observed. No diffraction peak corresponding to the carbon network was observed due to its low content.

Field emission-scanning electron microscopy (FE-SEM) images of $LiFePO_4$/C composite material are shown in Fig. 3. These images show a very interesting structural change when the sintering period increases from 2 to 20 h. The $LiFePO_4$/C composite network synthesized at 650 °C for 2 h shows a highly loose porous structure (Fig. 3a). On the other hand, the $LiFePO_4$/C composite network

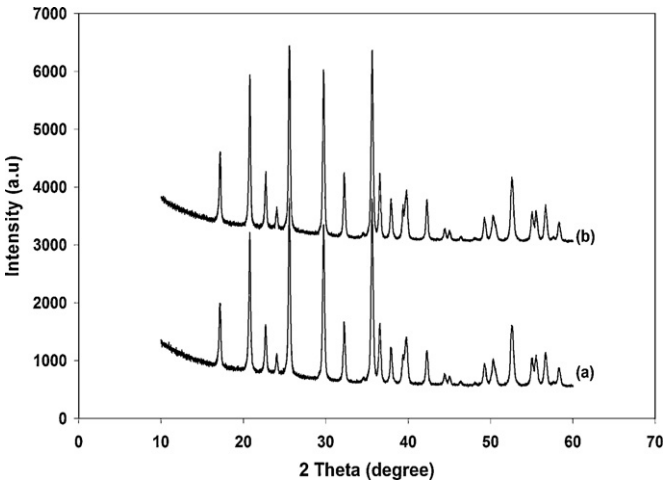

Fig. 2. X-ray diffraction patterns of $LiFePO_4$/C composite cathode material sintered at 650 °C at different sintering time: (a) 2 h and (b) 20 h.

transfers to a rod-like $LiFePO_4$/C composite material when the sintering time increased to 20 h (Fig. 3b and c). The low magnification image (Fig. 3b) clearly shows that the particles are mainly rod-like structure. The high magnification image (Fig. 3c) demonstrates the well-formed rod-like morphology of the $LiFePO_4$/C composite. This transformation process is related to the carbon decomposition (surface carbon) and volume shrinkage of hard carbon transformation process (interior carbon). The carbon in the interior of $LiFePO_4$/C composite aggregation transfer to hard carbon and shrunk the aggregation to form a dense rod-like $LiFePO_4$/C composite structure. The dense rod-like $LiFePO_4$/C composite structure transformation process agrees well with the TGA analysis result. Thus, it is reasonable to suggest that the transformation of the composite material

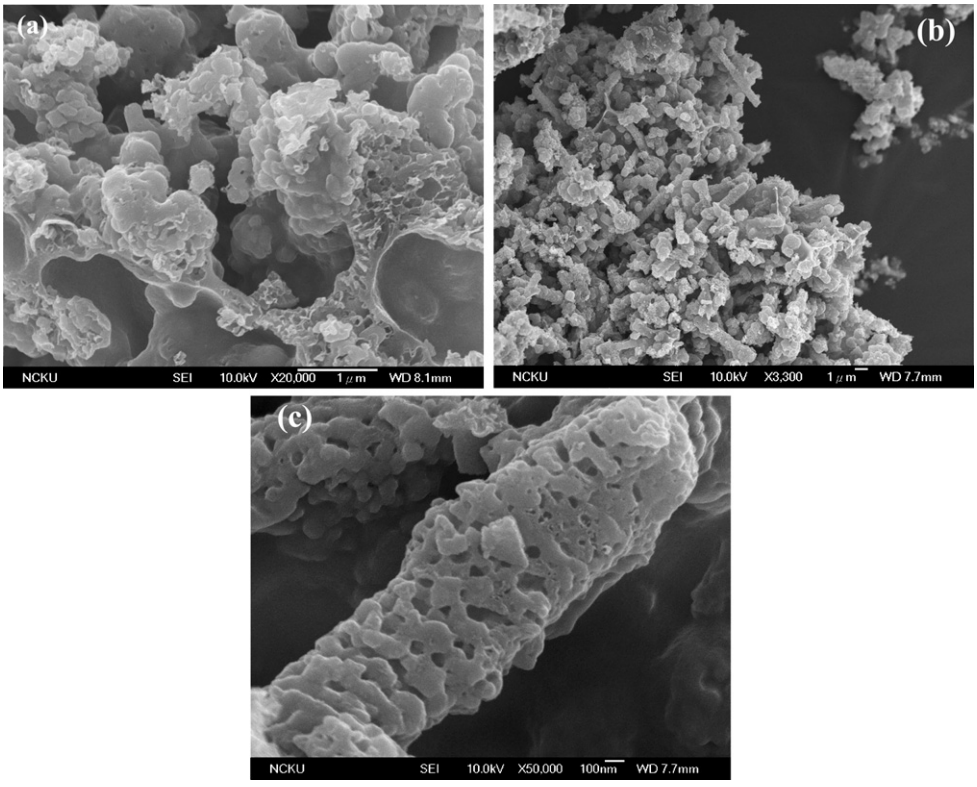

Fig. 3. Scanning electron microscopy (SEM) images of $LiFePO_4$/C composite cathode material sintered at 650 °C at different sintering time: (a) 2 h and (b and c) 20 h at low and high magnifications, respectively.

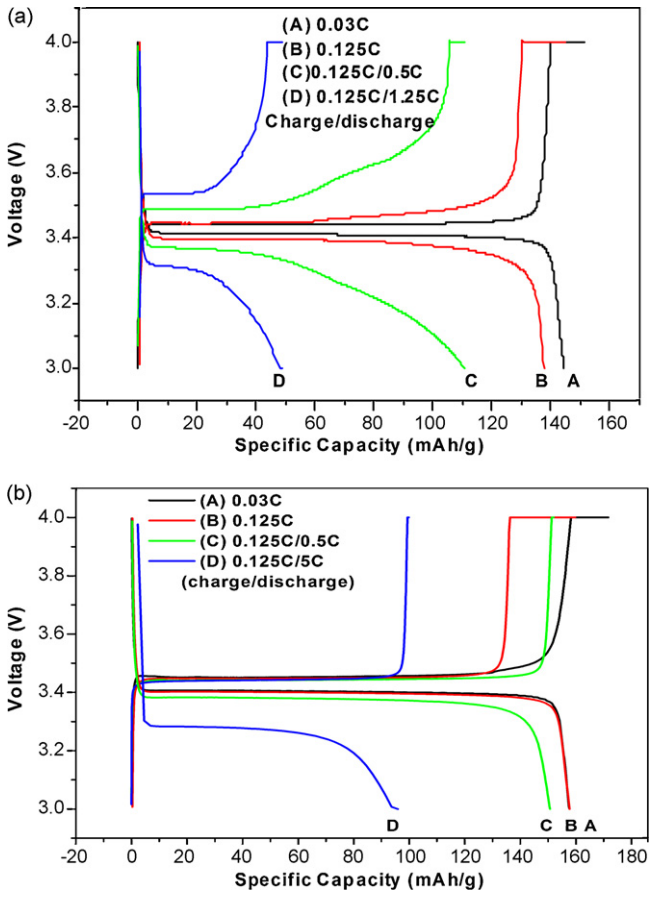

Fig. 4. Typical charge and discharge profiles of (a) loose porous and (b) rod-like $LiFePO_4$/C composite cathode materials at different C-rates.

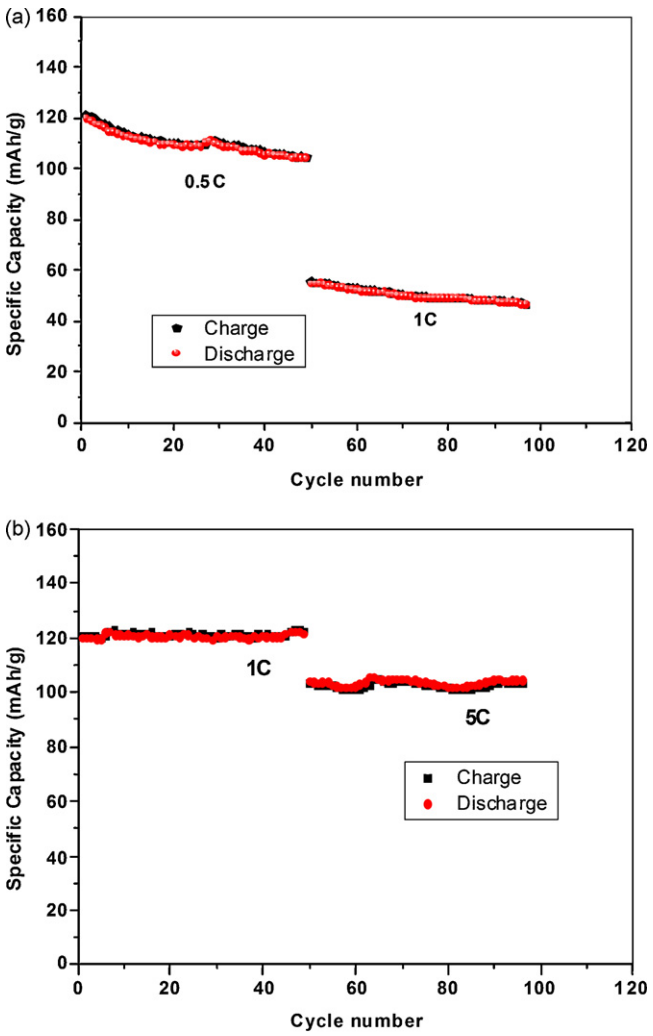

Fig. 5. Reversible charge and discharge specific capacities of (a) loose porous and (b) rod-like $LiFePO_4$/C composite cathode material during continuous cycling at different C-rates.

from loose porous structure to dense rod-like structure is indeed due to the volume shrinkage during hard carbon formation process. From the SEM image (Fig. 3b), one can clearly see that the rod-like $LiFePO_4$/C composite material formed by reverse micelle process consists of primary nanoparticles. This geometry has several advantages such as better accommodation of volume changes without fracture during cycling, better electrical connection with the current collector, and efficient electron transport.

The electrochemical performance of both porous and rod-like $LiFePO_4$/C composite material was investigated with lithium insertion/deinsertion process. High-rate properties of the composite materials were characterized for potential applicability in high-rate lithium ion batteries. Fig. 4 shows the typical charge/discharge profiles of loose porous (Fig. 4a) and rod-like (Fig. 4b) structured cathode material, respectively, at different discharge C-rates within a potential window of 3.0–4.0 V Vs Li at room temperature. The rod-like $LiFePO_4$/C composite material has a higher discharge capacity of 160 mAh g^{-1} at 0.03 C. This value is 10% greater than that of the porous $LiFePO_4$/C composite material (144 mAh g^{-1}). The high-rate performance of the rod-like material is indeed interesting since electron transfer at high C-rates would be a critical issue. Superior behaviors of rod-like $LiFePO_4$/C composite material are revealed, especially at higher C-rates. Specific capacities of 150 and 95 mAh g^{-1} are obtained at 0.5 and 5 C (Fig. 4b), respectively, for the rod-like material, whereas the specific capacities are 110 mAh g^{-1} at 0.5 C and 49 mAh g^{-1} at 1 C for the porous material (Fig. 4a). Fig. 5a and b shows cycling performance of loose porous material at 0.5 and 1 C, and rod-like material at 1 and 5 C, respectively. The rod-like material can deliver higher capacity under high-rate conditions as well as maintaining excellent capacity retention (Fig. 5b) when comparing to that of loose porous material (Fig. 5a). It is clearly seen that the discharging capacity remains stable at even 5 C for the rod-like material. The excellent performance of rate capability demonstrates the advantage of the synthesized nanostructured rod-like $LiFePO_4$/C cathode material to use in high-rate lithium ion batteries. We believe that the better discharge capacity and rate capability are greatly associated with unique rod-like composite material formed by primary nanoparticles. Since primary particles are held by relatively weak secondary bonds in the synthesized nanostructured rod-like $LiFePO_4$/C cathode material, the volume changes involved during insertion and deinsertion of lithium can readily be accommodated by relaxation of the binding force among primary particles [30]. Thus, the material remains intact with the current collector without breaking into smaller particles. Similar improvements in the electrochemical property of nanoscale grains and nanoscale structures in the spherical layered cathode material have been reported previously [31,32]. In addition, the rod-like $LiFePO_4$/C morphology would also increase the contact surface between the electrolyte and electrode resulting enhanced the cell performance. Hence, the rod-like nanostructured morphology not only improves the structural stability of the electrode, but also expected to improve the overall performance of the lithium ion battery. In addition, in comparison with the results reported previously for bare and modified $LiFePO_4$ powders [33,11,34] the rod-like

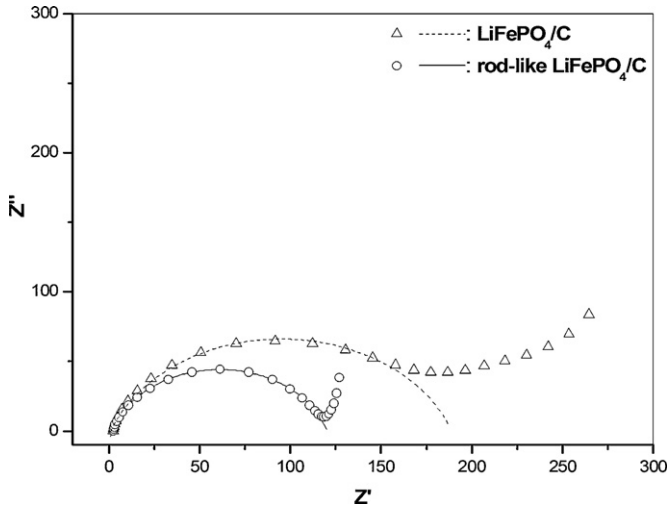

Fig. 6. Nyquist plots of loose porous and rod-like $LiFePO_4$/C composite cathode materials fitted with an equivalent circuit model.

$LiFePO_4$/C composite material prepared by template-free reverse micelle process, exhibited higher discharge capacity and rate capability due to improved structural stability, lithium ion diffusion and electronic conductivity.

In general, the difference in battery performances would be related to the interface reaction between positive electrode and the electrolyte [35–37]. To explore the reason for the enhanced electrochemical performance, AC impedance measurements were performed for the loose porous and rod-like $LiFePO_4$/C composite materials under open circuit voltage (OCV) conditions. One can clearly notice a significant difference in the impedance spectra between the materials with different morphologies as shown in Fig. 6. By comparing the diameter of the semicircles, the impedance of the porous material (187 Ω) is significantly larger than that of rod-like material (120 Ω). Warburg impedance is associated with the diffusion impedance of the species, which appears as a straight line in low frequency region during EIS analysis. Theoretically, the slope for Warburg impedance should be unity ($\theta = 45^\circ$), and not effected by other factors [38]. In the study of $LiMn_2O_4$ film electrodes by Jung and Pyun [39], they found that smooth thin film shows the unity slope ($\theta = 45^\circ$) in the Warburg impedance region. However, the slope for fractal electrodes shows obvious deviation to unity. The reason is owing to the surface morphology of the electrode. In our EIS analysis, the slopes observed for the two different materials are not identical, indicating the difference of the surface properties (shape, roughness) between rod-like and loose porous electrodes. Therefore, it is reasonable that the improved battery performances of rod-like $LiFePO_4$/C composite material is related to lower surface film resistance for the charge transfer process [40] and also lower surface area [41] when comparing with that of porous $LiFePO_4$/C composite material.

4. Conclusion

In summary, we have developed a simple and cost-effective template-free reverse micelle process for the synthesis of the rod-like $LiFePO_4$/C composite cathode material. This process demonstrates the ability to manipulate the shape and size of the composite cathode material. This approach yields secondary rod-like particles which are robust aggregates of primary nanoparticles. The size of the primary particles could be controlled based on the sintering time, whereas the size of the large aggregates is adjustable based on the carbon content of the composite. A possible mechanism has been proposed illustrating the role of both the confined space presented by template-free reverse micelle process as well as the importance of the carbon network-$LiFePO_4$ interactions leading to the formation of the large aggregates. The as-synthesized rod-like $LiFePO_4$/C composite material exhibits superior discharge capacity and rate capability when used as cathode materials in lithium batteries. Template-free reverse micelle process developed in this work opens up a new strategy to design better cathode materials, under controlled experimental conditions, with unique morphologies for future applications.

References

[1] G.A. Nazzri, G. Pistoia, Lithium Batteries: Science and Technology, Kluwer Academic/Plenum, Boston, 2004.
[2] J.M. Tarascon, M. Armond, Nature 414 (2001) 359.
[3] M.S. Whittingham, Chem. Rev. 104 (2004) 4271.
[4] H.K. Liu, G.X. Wang, Z. Guo, J. Wang, K. Konstantinov, J. Nanosci. Nanotechnol. 6 (2006) 1.
[5] A.K. Padhi, K.S. Nanjundaswamy, J.B. Goodenough, J. Electrochem. Soc. 144 (1997) 1188.
[6] A.K. Padhi, K.S. Nanjundaswamy, C. Masquelier, S. Okada, J.B. Goodenough, J. Electrochem. Soc. 144 (1997) 1609.
[7] A.S. Anderson, B. Kalska, L. Hggstrm, J.O. Thomas, Solid State Ionics 130 (1997) 41.
[8] H. Huang, S.C. Yin, L.F. Nazar, Electrochem, Solid State Lett. 4 (2001) A170.
[9] Z. Chen, J.R. Dahn, J. Electrochem. Soc. 149 (2002) A1184.
[10] S. Yang, Y. Song, P.Y. Zavalij, M.S. Whittingham, Electrochem. Commun. 4 (2002) 239.
[11] S.Y. Chung, J.T. Bloking, Y.M. Chiang, Nat. Mater. 1 (2002) 123.
[12] P.S. Herle, B. Ellis, N. Coombs, L.F. Nazar, Nat. Mater. 3 (2004) 147.
[13] G.X. Wang, S. Bewlay, S.A. Needham, H.K. Liu, R.S. Liu, V.A. Drozd, J.F. Lee, J.M. Chen, J. Electrochem. Soc. 153 (2006) A25.
[14] G. Meligrana, C. Gerbaldi, N. Penazzi, J. Power Sources 160 (2006) 516.
[15] K.F. Hsu, S.Y. Tsay, B.J. Hwang, J. Mater. Chem. 14 (2004) 2690.
[16] K.F. Hsu, S.Y. Tsay, B.J. Hwang, J. Power Sources 192 (2009) 660.
[17] A. Yamada, S.C. Chung, K. Hinokuma, J. Electrochem. Soc. 148 (2001) A224.
[18] D.H. Kim, J. Kim, Electrochem. Solid State Lett. 9 (2006) A439.
[19] C.W. Kim, M.H. Lee, W.T. Jeong, K.S. Lee, J. Power Sources 146 (2005) 534.
[20] S.T. Myung, S. Komaba, N. Hirosaki, H. Yashiro, N. Kumagai, Electrochim. Acta 49 (2004) 4213.
[21] K. Konstantinov, S. Bewlay, G.X. Wang, M. Lindsay, J.Z. Wang, Electrochim. Acta 50 (2004) 421.
[22] I. Belharouak, C. Johnson, K. Amine, Electrochem. Commun. 7 (2005) 983.
[23] K.S. Park, J.T. Son, H.T. Chung, S.J. Kim, C.H. Lee, H.G. Kim, Electrochem. Commun. 5 (2003) 839.
[24] M. Antonietti, C. Goltner, Angew. Chem. Int. Ed. Engl. 36 (1997) 910.
[25] S. Mann, Biomimetic Materials Chemistry, VCH, New York, 1996.
[26] M. Nishizawa, K. Mukai, S. Kuwabata, C.R. Martin, H. Yoneyama, J. Electrochem. Soc. 144 (1997) 1923.
[27] C.J. Patrissi, C.R. Martin, J. Electrochem. Soc. 146 (1999) 3176.
[28] C.J. Patrissi, C.R. Martin, J. Electrochem. Soc. 148 (2001) A1247.
[29] Z. Sun, X. Shi, X. Wang, Y. Sun, Diamond Relat. Mater. 8 (1999) 1107.
[30] H. Park, H.S. Shin, S.T. Myung, C.S. Yoon, K. Amine, Y.K. Sun, Chem. Mater. 6–8 (2005) 17.
[31] M. Chiang, H. Wang, Y.I. Jang, Chem. Mater. 13 (2001) 53.
[32] S.H. Kang, J.B. Goodenough, L.K. Rabenberg, Chem. Mater. 13 (2001) 1758.
[33] F. Croce, A.D. Epifanio, J. Hassoun, A. Deptula, T. Olczac, B. Scrosati, Electrochem, Solid State Lett. 5 (2002) A47.
[34] K. Stribel, A. Guerfi, J. Shim, M. Armand, M. Gauthier, K. Zahib, J. Power Sources 119–121 (2003) 951.
[35] Y.M. Cho, S.I. Pyun, Solid State Ionics 99 (1997) 173.
[36] S.M. Lee, S.H. Oh, W.I. Cho, H. Jang, Electrochim. Acta 52 (2006) 1507.
[37] J. Ying, C. Wan, C. Jiang, J. Power Sources 102 (2001) 162.
[38] A.J. Bard, L.R. Faulkner, Electrochemical Methods: Fundamentals and Applications, 2nd ed., John Wiley & Sons, New York, 2000.
[39] K.N. Jung, S.I. Pyun, Electrochim. Acta 51 (2006) 4649.
[40] K. Dokko, M. Mohamedi, Y. Fujita, T. Itoh, M. Nishizawa, M. Umeda, I. Uchida, J. Electrochem. Soc. 148 (2001) A422.
[41] T.H. Cho, S.M. Park, M. Yoshio, T. Hirai, Y. Hideshima, J. Power Sources 142 (2005) 306.